Developmental Biology 386 (2014) 358–370

Contents lists available at ScienceDirect

Developmental Biology

journal homepage: www.elsevier.com/locate/developmentalbiology

MicroRNA-9 promotes the switch from early-born to late-born motor neuron populations by regulating Onecut transcription factor expression ☆

Georg Luxenhofer [a,1], Michaela S. Helmbrecht [a,*,1], Jana Langhoff [a], Sebastian A. Giusti [b], Damian Refojo [b], Andrea B. Huber [a,*]

[a] Institute of Developmental Genetics, Helmholtz Zentrum München – German Research Center for Environmental Health, Ingolstaedter Landstr. 1, 85764 Neuherberg, Germany
[b] Max Planck Institute of Psychiatry, Kraepelinstr. 2-10, 80804 Munich, Germany

ARTICLE INFO

Article history:
Received 2 September 2013
Received in revised form
11 December 2013
Accepted 13 December 2013
Available online 24 December 2013

Keywords:
Motor neuron development
MicroRNA-9
Onecut

ABSTRACT

Motor neurons in the vertebrate spinal cord are stereotypically organized along the rostro-caudal axis in discrete columns that specifically innervate peripheral muscle domains. Originating from the same progenitor domain, the generation of spinal motor neurons is orchestrated by a spatially and temporally tightly regulated set of secreted molecules and transcription factors such as retinoic acid and the Lim homeodomain transcription factors Isl1 and Lhx1. However, the molecular interactions between these factors remained unclear. In this study we examined the role of the microRNA 9 (miR-9) in the specification of spinal motor neurons and identified Onecut1 (OC1) as one of its targets. miR-9 and OC1 are expressed in mutually exclusive patterns in the developing chick spinal cord, with high OC1 levels in early-born motor neurons and high miR-9 levels in late-born motor neurons. miR-9 efficiently represses OC1 expression in vitro and in vivo. Overexpression of miR-9 leads to an increase in late-born neurons, while miR-9 loss-of-function induces additional OC1$^+$ motor neurons that display a transcriptional profile typical of early-born neurons. These results demonstrate that regulation of OC1 by miR-9 is a crucial step in the specification of spinal motor neurons and support a model in which miR-9 expression in late-born LMCl neurons downregulates Isl1 expression through inhibition of OC1. In conclusion, our study contributes essential factors to the molecular network specifying spinal motor neurons and emphasizes the importance of microRNAs as key players in the generation of neuronal diversity.

Introduction

In the developing neural tube numerous transcription factors act in concert to generate a large diversity of neurons that eventually will populate the mature spinal cord in stereotypic patterns. Precursors within the ventricular pMN domain first give rise to motor neurons of the medial motor column (MMC) and the medial aspect of the lateral motor column (LMCm) before motor neurons of the lateral LMC (LMCl) are generated (Jessell, 2000). Several genetic determinants for the establishment of columnar motor neuron identity have been identified. For example, the maintenance of Isl1 expression by Onecut transcription factors is important to generate LMCm neurons. Later during spinal cord development cross-repressive interactions between Isl1 and another transcription factor, Lhx1, lead to the formation of lateral LMC neurons (Francius and Clotman, 2009; Roy et al., 2012; Kania and Jessell, 2003). While the generation of Lhx1$^+$ LMCl neurons is dependent on retinoic acid secreted from early-born LMCm neurons (Sockanathan and Jessell, 1998; Sockanathan et al., 2003), the regulatory events downstream of retinoic acid signaling and upstream of the Isl1/Lhx1 cross-repressive events are unclear.

It is now appreciated that posttranscriptional silencing by microRNAs plays an important role in the spatial and temporal regulation of neuronal specification (Shi et al., 2010). Indeed, disrupting microRNA biogenesis by conditional deletion of Dicer in motor neuron progenitors caused loss of many limb and sympathetic ganglia-innervating spinal motor neurons (Chen and Wichterle, 2012; Zheng et al., 2010). Recently, miR-9 was found to regulate the formation of divisional identity by fine-tuning expression levels

* Corresponding authors.
E-mail addresses: michaela.helmbrecht@helmholtz-muenchen.de (M. S. Helmbrecht), andrea.huber@helmholtz-muenchen.de (A.B. Huber).

[1] These authors contributed equally.

0012-1606/$ - see front matter © 2014 The Authors. Published by Elsevier Inc. All rights reserved.
http://dx.doi.org/10.1016/j.ydbio.2013.12.023

of FoxP1, a transcription factor involved in the generation of lateral motor column (LMC) motor neurons and motor neurons of the preganglionic motor column (PGC; (Otaegi et al., 2011). The expression pattern and function of miR-9 during maturation and specification of brachial motor neurons, however, suggest that beside the modulation of FoxP1 levels miR-9 may play an additional role in the establishment of motor neuron subtypes.

Here, we show that miR-9 and OC1 are expressed in mutually exclusive patterns within the LMC and MMC. Using gain- and loss-of-function approaches we demonstrate that miR-9 controls OC1 protein expression. In addition, our results show that miR-9 promotes the generation of later-born motor neurons while miR-9 knockdown leads to the transcriptional profile of early-born motor neurons. Our data support a role of miR-9 in the specification of motor neuron subtypes through the modulation of OC1 function.

Materials and methods

Chick electroporation

Fertilized eggs were stored at 10–15 °C and incubated for 2 days at 37.5 °C. In ovo electroporation was performed at HH St 10–14 by injecting respective DNA/RNA dissolved in PBS and 0.01% Fast Green into the central canal of the spinal cord. Unilateral transfection was performed using a platinum electrode (CUY 610P4-4, Sonidel, USA) and 5 pulses of 25 V (duration 50 ms each) using a BTX ECM830 square wave electroporator (Harvard apparatus, Edenbridge, UK). After electroporation, eggs were incubated again at 37.5 °C. At the appropriate time points embryos were removed, staged, and fixed with 4% PFA at 4 °C.

DNA/RNA constructs

For miR-9 gain-of-function experiments, Ambion® Pre-miR-9 and negative control Pre-miR miRNA precursors (Life Technologies, Darmstadt, Germany) were used at a final concentration of 5 μM. To control for efficiency of electroporations, a GFP expressing plasmid at a concentration of 0.3–0.5 μg/μl was co-electroporated.

The CAG-GFP-miR-9 sponge plasmid was constructed using a modified pCRII vector as backbone (Life Technologies) in which the CAG promoter was inserted via HindIII/SacI. The GFP cDNA sequence was PCR-amplified from a pEGFP-N1 vector (BD Biosciences, Heidelberg, Germany) and subcloned using the introduced SacI and the BamHI restriction sites. The microRNA sponge construct consisting of eighteen repetitive bulged complementary miR-9 sequences (5′-TCATACAGCTATATACCAAAGA-3′) separated by a variable four-nucleotide linker was chemically synthesized (GenScript Corp., Piscataway, NJ, USA) and introduced in the 3′UTR of GFP cDNA via BamHI/XhoI. For the scrambled sponge the sequence 5′-ATGATAA-CAACGAACGATTACAC-3′ was used. The BGH polyA signal was PCR-amplified from the pcDNA3 plasmid (Life Technologies) and introduced downstream of the sponge construct via XbaI/ApaI. The control plasmid pCAG-GFP was subsequently generated by removing the miR-9 sponge using BamHI and XhoI sites and religated after a Klenow fill-in. For the miR-9 luciferase sensor vector we used the pCRII backbone and cloned the CAG promoter upstream of the firefly luciferase gene containing an artificial 3′UTR with a single fully complementary binding site for miR-9 (sequence of the 3′UTR: 5′-GGATCCTCATACAGCTAGATAACCAAAGAGAGCTC-3′), followed by a BGH polyA.

To validate the interaction between miR-9 and OC1, two reporter Plasmids, pGL3-4xOC1ts and pGL3-cOC1-3′UTR were generated. pGL3-4xOC1ts was made by inserting a synthesized DNA sequence containing 4 repeats of the conserved miR-9 target sites of OC1 (DNA sequence) separated by 4 nt spacer into the XbaI sites of the pGL3 promotor vector (Promega, Mannheim, Germany). For the construction of pGL3-cOC1-3′UTR the chick OC1 3′UTR (466 bp) was amplified from chick E6 cDNA (forward primer: 5′-CGTCTAGACTTGTACCAAAGCATGAAGG-3′; reverse primer: 5′-CGTCTAGACATGGACACACTGCACACCT-3′) and inserted into the pGL3 vector. The plasmid pcDNA6.2 EmGFP miR-9 (obtained from Lynn Hudson, Addgene plasmid 22741; (Lau et al., 2008) was used to overexpress miR-9 in HEK293T cells.

Immunohistochemistry and in situ hybridization

For immunohistochemical analysis, fixed chick embryos were cryoprotected in 30% sucrose at 4 °C and embedded in TissueTek (Sakura, Alphen, The Netherlands). Immunostaining on tissue sections (12 μm) was performed as described before (Huber et al., 2005) with the modification that prior to antibody incubation cryosections were placed in hot (95–100 °C) antigen retrieval solution (1 mM Tris, 5 mM EDTA, pH 8.0). After cooling down for 20 min, sections were washed twice in PBS before proceeding with the standard blocking step. For immunohistochemistry the following primary antibodies were used: anti-hFoxP1 (1:500, R&D Systems, Wiesbaden, Germany), anti-Hnf6 (clone H-100, 1:500, Santa Cruz Biotechnology, Heidelberg, Germany), chick-anti-GFP (1:1000, Aves Labs, Oregon, USA). The following antibodies were developed by T.M. Jessell and obtained from the Developmental Studies Hybridoma Bank under the auspices of the NICHD and maintained by The University of Iowa, Department of Biology, Iowa City, IA 52242: anti-Isl1/2 (39.4D5, 1:100), anti-Isl1 (39.3F7, 1:100), anti-Hb9 (81.5C10, 1:100), anti-Neurofilament (3A10, 1:50) and anti-Lhx3 (67.4E12, 1:100). The polyclonal rabbit anti Lhx-1 antiserum was raised against an Lhx1-specific peptide (GNHLSHPPEM-NEAAVW) as reported before (Tsuchida et al., 1994) and used at a dilution of 1:2000.

Expression of miR-9 was detected with anti-miR-9 LNA detection probes (Exiqon, Vedbaek, Denmark) labeled with digoxigenin using 2nd generation dig labeling kit (Roche Diagnostics, Mannheim, Germany). Fixed 12 μm tissue sections were deacetylated for 10 min in 1% Triethanolamin and 0.125% acetic anhydride and treated with Proteinase K (5 μg/ml in PBS) for 5 min. Hybridization was performed over night at 52 °C with a dilution of 1:2000 of labeled miR-9 detection probe in hybridization buffer (50× Formamid, 5× SSC, 5× Denhardt's solution, 200 μg/μl torula yeast RNA). Subsequent to hybridization, stringent washing steps were performed at 60 °C: 4×15 min 1× SSC+0.1% TritonX100, 4×15 min 0.2×SSC+0.1% TritonX100. After an additional washing step at room temperature with 0.2 1×SSC+0.1% Triton X100 for 15 min, the probe was detected with an AP tagged anti-digoxigenin antibody (Roche Diagnostics) as described by the manufacturer followed a NBT/BCIP chromogenic reaction (Roche Diagnostics).

Luciferase assay

For each transfection of HEK293T cells following amounts of plasmids were used: 20 ng of firefly luciferase expressing vector (pGL3, pGL3-4xOC1ts, pGL3-cOC1-3′UTR or miR-9-luciferase sensor vector), 5 ng of a renilla luciferase expressing vector (pRL-TK, Promega) and 50 ng miR-9 expressing or control vector (pcDNA6.1 EmGFP lacking miR-9). After transfection, cells were grown for 40–48 h, lysed and luciferase activity was detected using the reagents Beetle Juice and Renilla Juice (PJK, Kleinbittersdorf, Germany). Mean luciferase ratios (firefly luciferase/renilla luciferase) of triplicate experiments were normalized to control experiments with plasmids lacking miR-9 expression.

Double fluorescence GFP/RFP sensor assay

To validate miR-9 function cell autonomously in vivo we used a double fluorescence GFP/RFP sensor (DFRS) plasmid for miR-9 (Tonelli et al., 2006) in which two binding sites for miR-9 were introduced in the 3′UTR of the RFP coding sequence (DFRS-miR-9). To detect the baseline RFP/GFP ratio of the GFP reporter and the RFP sensor, the plasmid DFRS-miR-9mut was used in which the miR-9 binding sites were mutated. Plasmids were electroporated into chick spinal cord at HH St 12–14 and analyzed at HH St 27/28. A 12 μm cryosections were immunostained for Isl1 and Lhx1 to identify brachial LMCm and LMCl neurons and direct GFP and RFP signal was determined using identical microscope settings for all samples. The mean baseline RFP/GFP ratio of LMCm (1.54 ± 0.05, mean ± SEM, $n=81$ neurons from 2 embryos) and LMCl neurons (2.39 ± 0.11, $n=38$ from 2 embryos) was determined using the DFRS-miR-9mut plasmid and used to normalize the individual RFP/GFP ratio of LMCm and LMC neurons expressing the DFRS-miR-9 sensor, respectively.

Quantification of OC1 expression

To determine the OC1 immunfluorescence signal after miR-9 gain-of-function the mean fluorescence signal of individual neuronal nuclei was measured using ImageJ. The mean data of all examined neurons from the electroporated side of a 12 μm cryosection was then normalized to the control side of the same section and displayed as difference to control. In miR-9 knock down experiments OC1 signal intensity of individual GFP^+ nuclei from miR-9 sponge or control electroporated neurons was measured with ImageJ and mean intensities were calculated and compared.

Tracing experiments

Retrogade tracing experiments were performed in HH St 29–30 chick embryos. Chick embryos were removed and eviscerated in oxygenated DMEM/F12 (Life Technologies). 6% Tetramethylrhodamin or Alexa488 conjugated dextran (Life Technologies) in 0.4% TritonX100/PBS was injected into longus colli or semispinalis cervicis muscles using fine pointed glass capillaries. Subsequently, embryos were incubated for 3–5 h in oxygenated DMEM/F12 before fixation and further processing.

Determination of axon branch thickness

To determine the thickness of ventral and dorsal axon branches, whole embryos were immunostained against neurofilament and GFP as described (Huber et al., 2005). Axon branches innervating electroporated and control wings were imaged using confocal laser scanning microscopy (LSM 510, Zeiss, Jena, Germany) at identical positions. 25 μm confocal stacks of either radial nerve or ulnar and median nerves were collapsed onto a single plane and branch thickness was determined by an experimenter blinded to the experimental conditions. Radial nerve thickness was measured at a distance of 100 μm proximally to the stereotypic bifurcation (see Fig. 6B), while ulnar and median nerve thickness was determined 200 μm distally to the point where the nerves separate (see Fig. 6B). Values of the electroporated wing were normalized to values of the non-electroporated control side and values of ulnar and median nerve were summarized to obtain the thickness of the ventral nerve branch.

Determination of motor neuron identity

Brachial motor columns were determined using immunostainings against Isl1, FoxP1, Lhx1, Hb9 and Lhx3. $Isl1^+/FoxP1^+$ cells were counted as LMCm neurons, $Lhx1^+/Hb9^+$ cells or $Isl1^-/FoxP1^+$ cells were assigned to the LMCl. Due to incompatible Lhx3 and Hb9 antibodies, $Lhx3^+$ cells were classified as MMC neurons if positioned in Hb9-positive area of the adjacent cryosection. To determine differences in motor neuron numbers, respective cell numbers of the non-electroporated side were subtracted from the electroporated side and normalized to the control cell number ([EP cell # – control cell #]/control cell#) for each cryosection. The transcriptional profile of GFP^+ neurons was determined using immunostainings against the motor column markers described above.

Statistical analysis

Statistical analysis was performed using Prism5 (GraphPad Software, LaJolla, CA, USA). A Wilcoxon sign ranked test was performed to determine significant differences in neuronal numbers and OC1 expression in miR-9 gain-of-function experiments. Luciferase assays were analyzed by a one-way ANOVA with Tukey's multiple comparison post-hoc test. For the evaluation of GFP^+ cell identity a Mann–Whitney test was used. A Student's *t*-test was performed in DFRS experiments and in the evaluation of OC1 signal intensity after miR-9 knock down.

Results

MicroRNA-9 is expressed differentially in brachial motor columns

We first examined the expression patterns of miR-9 in postmitotic motor neurons in the brachial spinal cord at HH St 20 to 28, when motor neurons are generated and establish their peripheral projections. During motor axon outgrowth very little miR-9 expression is detectable in the chick spinal cord (Fig. 1A). One day later, at HH St 25, miR-9 levels increase in ventricular and intermediate zones of the spinal cord (Fig. 1B), similar to previous observations (Darnell et al., 2006; Zheng et al., 2010). At HH St 28, when motor neuron migration is almost complete, and the medial motor column (MMC) as well as lateral and medial aspects of the lateral motor column (LMCl and LMCm) can be clearly distinguished by position and molecular markers, miR-9 is expressed in specific subpopulations of motor neurons (Fig. 1C). To identify individual motor columns in the brachial spinal cord and assign the miR-9 in situ hybridization signal to specific motoneuronal populations, we stained adjacent sections with either Isl1/FoxP1 (LMCm), Lhx1/Hb9 (LMCl) and Lhx3 (MMC). LMC neurons exhibit different levels of miR-9 expression depending upon whether they innervate dorsal or ventral limb muscles. Throughout the brachial spinal cord, LMCl neurons that innervate dorsal limb muscles show stronger miR-9 expression than LMCm neurons projecting to ventral limb muscles (Fig. 1, Fig. S1). To evaluate whether this differential expression is also manifested in a differential functional activity of miR-9, we electroporated a double fluorescence GFP reporter/RFP miR-9 sensor plasmid (DFRS miR-9, (Tonelli et al., 2006) into the chick spinal cord. In this construct both fluorescent proteins are expressed under the same promoter but only the 3′UTR of RFP contains two miR-9 target sites. Thus, functionally active miR-9 causes a downregulation of the RFP signal in electroporated cells, while the GFP signal is not affected. Using this assay we were able to evaluate miR-9 function by measuring the RFP/GFP ratio. We found that the RFP/GFP ratio was 40% lower in LMCl neurons when compared to medial LMC

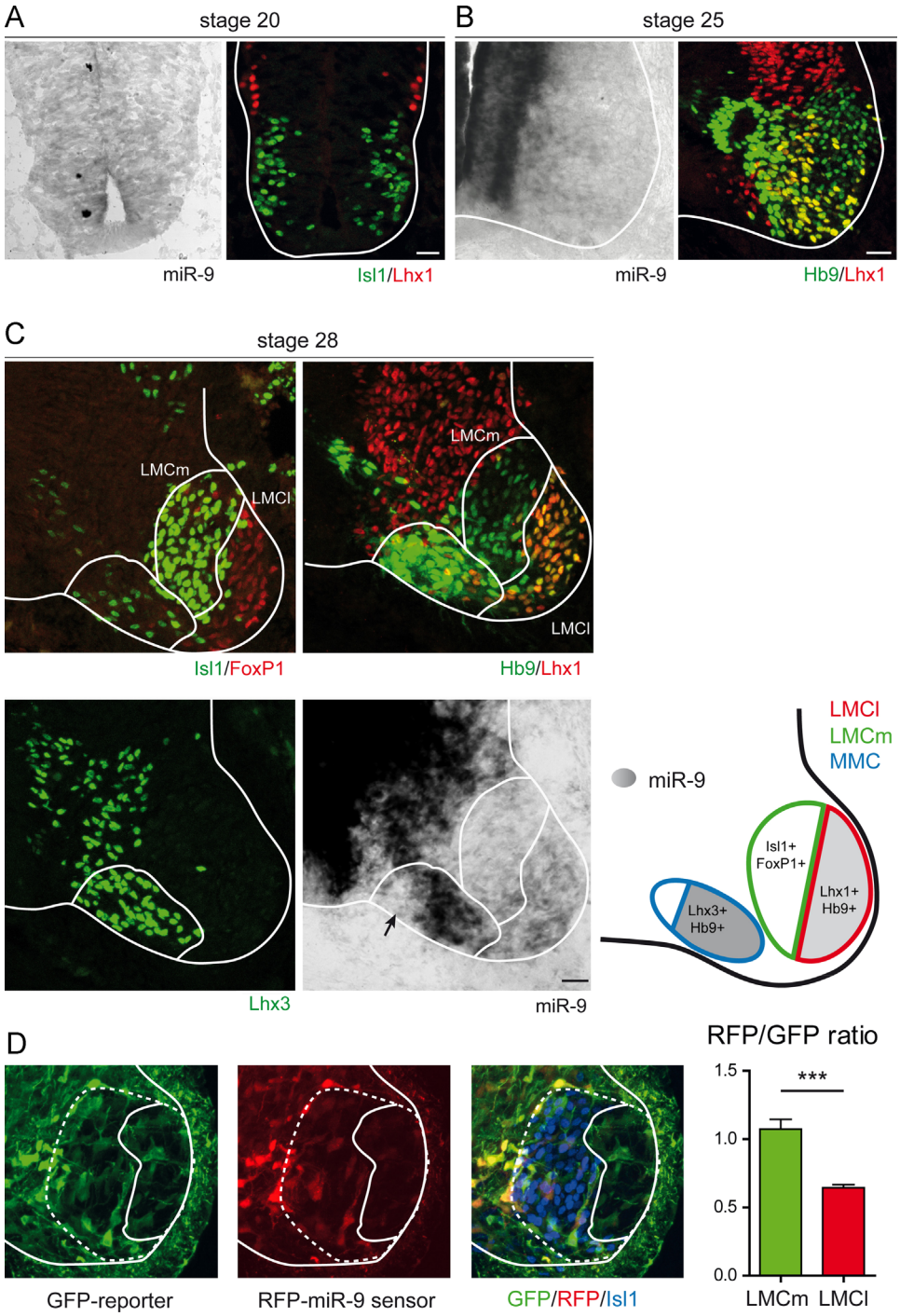

Fig. 1. Expression of miR-9 in the developing spinal cord. (A) Expression of miR-9 is almost not present at early developmental stages (HH St 20). (B) miR-9 strongly increases at HH stage 25 in the ventricular zone and is also present in Hb9$^+$ motor neurons. (C) At HH St 28, brachial lateral motor column (LMC) divisions were identified with Isl1/FoxP1 (LMCm) and Lhx1/Hb9 (LMCl). Brachial MMC motor neurons were identified as Lhx3$^+$ neurons located in the Hb9 area of the adjacent section. Schematic drawing of miR-9 expression pattern at HH St28 visualizes miR-9 expression in the lateral LMC and lateral MMC. (D) Expression of a double fluorescence GFP reporter/ RFP miR-9 sensor (DFRS miR-9) plasmid and evaluation of the RFP/GFP ratio in individual LMCl and LMCl neurons. Lateral LMC neurons exhibit a significant lower RFP/GFP ratio (0.64 ± 0.02, mean $\pm$ SEM, $n=151$) than medial LMC neurons (1.07 ± 0.07, $n=81$, $p<0.0001$). Scale bars 20 μm.

neurons thereby demonstrating a higher level of functionally active miR-9 in LMCl neurons (Fig. 1D). Thus, combining histological and functional approaches, we showed that miR-9 is differentially expressed in the brachial LMC.

In MMC neurons, miR-9 expression is very strong in the lateral aspect of the MMC while it is absent in more medially located Lhx3$^+$ brachial spinal motor neurons (Fig. 1C, arrow). This differential miR-9 expression pattern is even more distinct at later developmental stages (Fig. 3B) and suggests a potential role for this microRNA in generating columnar identity.

miR-9 and the transcription factor Onecut exhibit mutually exclusive expression patterns

Members of the Onecut (OC) family of transcription factors are differentially expressed in the mouse and chicken spinal cord

(Francius and Clotman, 2009). Mouse OC1/2 3′UTRs contain several highly conserved miR-9 target sites and miR-9 regulation of OC1/2 expression has been validated in cortical neurons and in the pancreas (Bonev et al., 2011; Dajas-Bailador et al., 2012; Plaisance et al., 2006). The Onecut transcription factors have not yet been annotated in chicken genome and transcriptome assemblies. However, computational analysis suggests the presence of the OC1 gene on chromosome 10 (Francius and Clotman, 2009). In this study, an antibody against mouse OC1 (HNF-6) was used to investigate the expression pattern of chick OC1 at very early (HH St 18) and late (HH St 29) stages of chick spinal cord development. The authors found that OC1 is initially expressed by many motor neuron populations, while it becomes restricted to a specific subset of spinal motor neurons at later stages (Francius and Clotman, 2009). Here, we examined intermediate developmental stages (HH St 20–28) to determine the degree of correlation between OC1 and miR-9 expression profiles.

At HH St 20/21 virtually all mature motor neurons, which are located in the lateral aspect of the ventral horn, express OC1 as shown by co-labeling with Isl1/2 (Fig. 2A). One day later, OC1 expressing cells are Isl1$^+$/Lhx3$^+$ representing early-born MMC neurons (Fig. 2B, arrows). At this developmental stage, prospective Lhx1$^+$/Hb9$^+$ LMCl neurons are still migrating and are therefore positioned more medially with respect to LMCm neurons (Fig. 2B, asterisk). LMCm neurons express OC1 at significantly higher levels than LMCl neurons, which is even more prominent at HH St 27 (Fig. 2C). Lhx3$^+$ neurons located in medial areas of the MMC strongly express OC1 (Fig. 2C, arrows), while hardly any OC1 signal was detectable in lateral MMC neurons (Fig. 2C, asterisk). Thus, OC1 expression levels differ greatly between motor neuron subpopulations, with OC1 being strongly expressed in neurons in the LMCm and medial areas of the MMC, where only low miR-9 expression levels were found (Fig. 2C).

Taken together, the expression patterns of miR-9 and OC1 during the generation and maturation of spinal motor neurons are mutually exclusive. In the LMCm, where OC1 protein expression is strong at HH St 27/28, miR-9 is absent, whereas lateral LMC neurons display a low OC1 signal and a strong miR-9 expression (Fig. 2D). Such a complementary expression pattern was also found in the MMC.

At brachial spinal levels, MMC neurons innervate the semispinalis cervicis (SC) and the longus colli (LC) muscles (Gutman et al., 1993), however, at present there are no molecular markers that allow for identification of muscle-specific MMC pools. We therefore retrogradely traced motor neurons that innervate the LC and the SC muscles by injecting fluorescent dextran conjugates. Antibody labeling and in situ hybridization analyses revealed that the LC innervating MMC neurons (MMC$_{LC}$) are located medially and express OC1 and Lhx3 but not miR-9 (Fig. 3A and B). In contrast, motor neurons innervating the

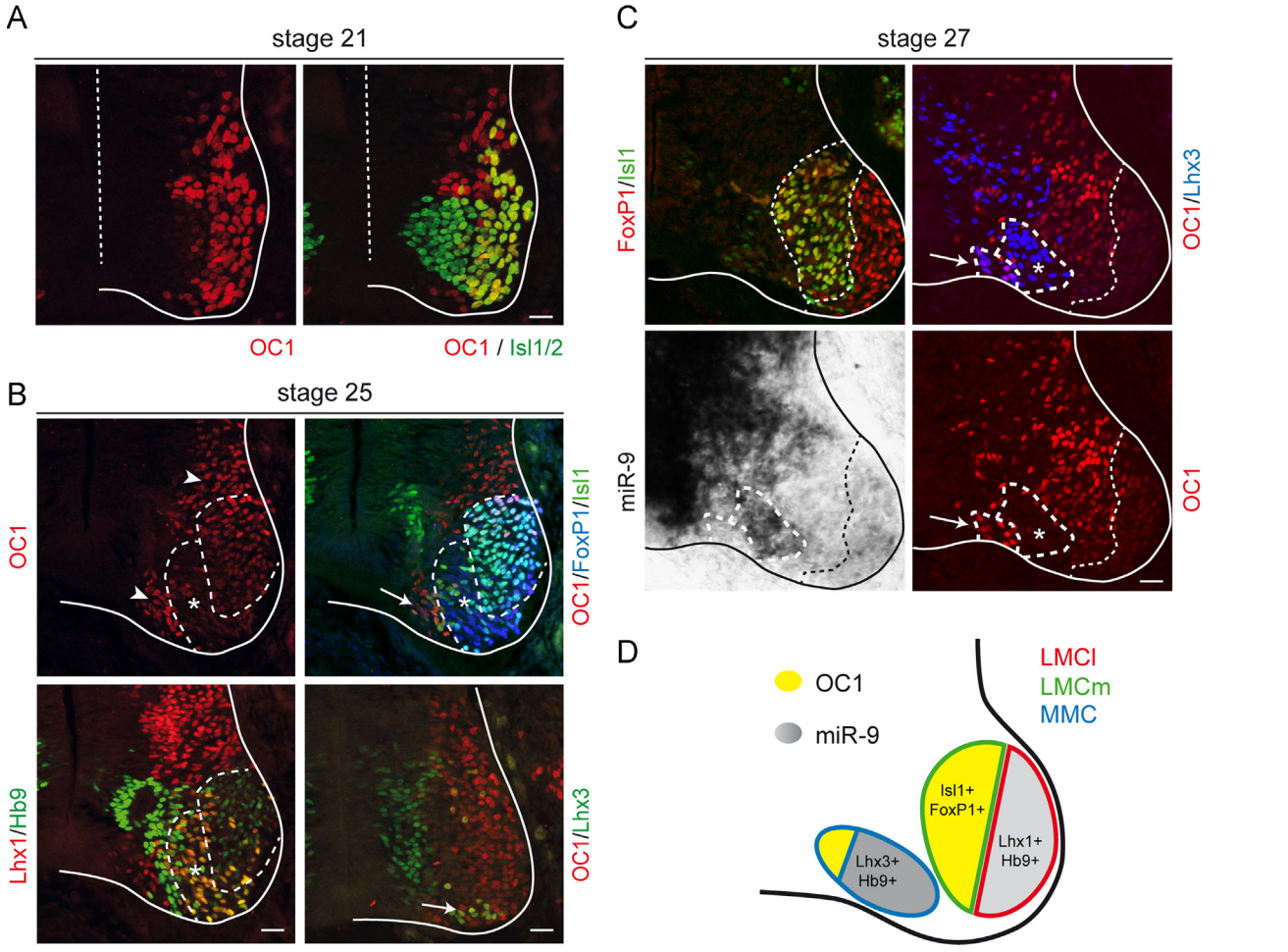

Fig. 2. Onecut1 expression pattern in the brachial spinal cord. (A) At early stages (HH St 21) Onecut1 is expressed in all mature Isl1/2-positive motor neurons, which are already located in a lateral position of the ventral horn. (B) At HH St 25, OC1 expression gets restricted to dorsolateral and medioventral positions (arrowheads). Newly born Lhx1/Hb9 double-positive LMCl neurons downregulate OC1 (asterisk). Early-born Lhx3$^+$/OC1$^+$ neurons reside at a very medioventral position (arrow). (C) At HH St 27, late-born Lhx3$^+$ MMC neurons (asterisk) do not express OC1, and migrate laterally compared to the early born Lhx3$^+$/OC1$^+$ MMC neurons (arrows). Isl1/FoxP1 double-positive LMCm neurons express high levels of OC1 while Isl1-negative LMCl neurons are devoid of OC1. (D) Comparison of OC1 and miR-9 expression within the brachial ventral horn. Areas of high OC1 and high miR-9 expression are mutually exclusive. LMCm and medial parts of the MMC exhibit low or absent miR-9 expression but are occupied by OC1^{high} neurons, while neurons in the lateral part of the MMC and in the LMCl express miR-9 but not OC1. Scale bars 20 μm.

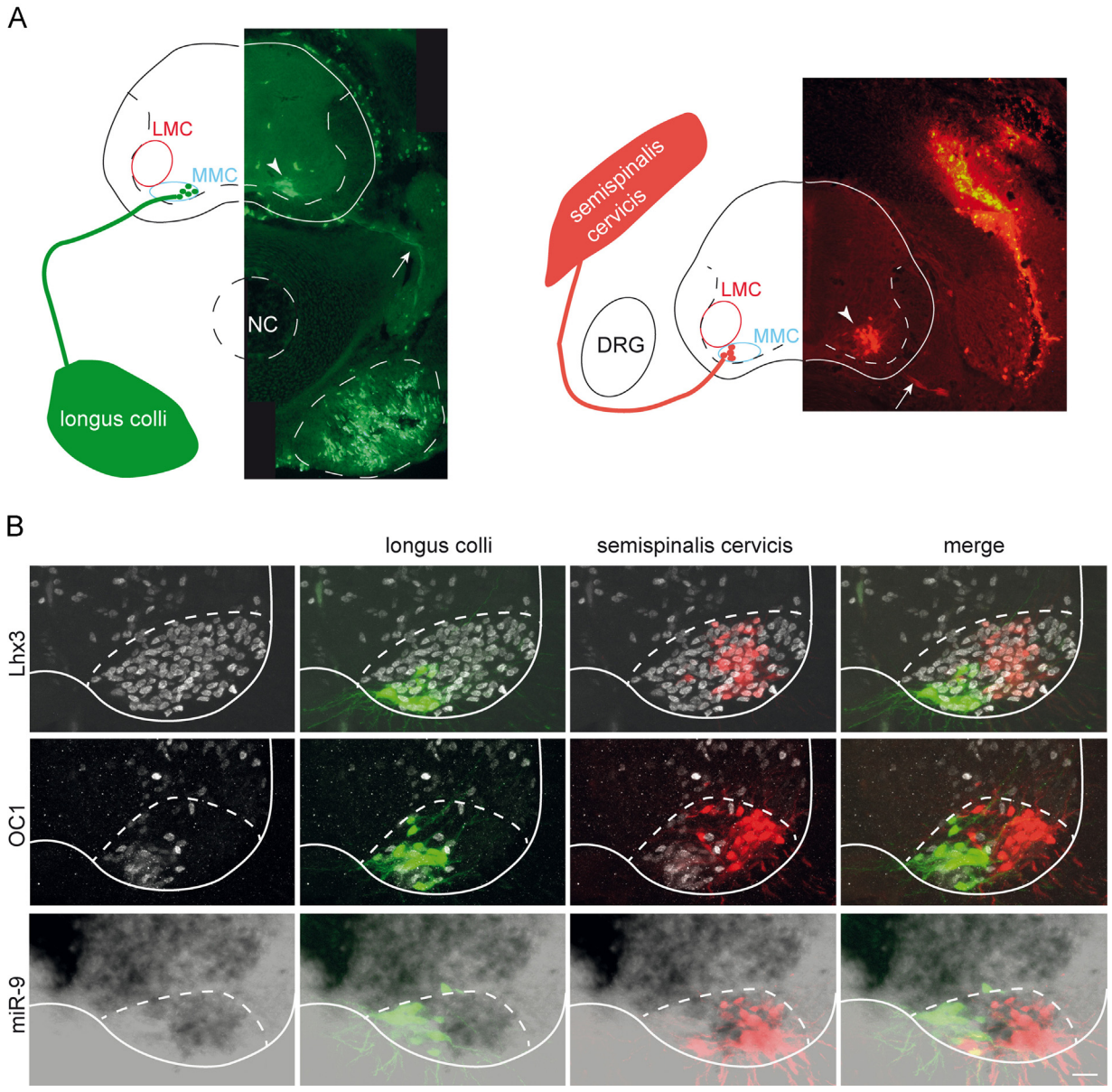

Fig. 3. Retrograde tracing from longus colli and semispinalis cervicis muscles. (A) Visualization of retrograde tracings of longus colli (LC) or semispinalis cervicis (SC) muscles with Alexa488 or Rhodamin coupled dextran, respectively, in coronal sections of HH St 29/30 embryos. Motor neurons in the medioventral aspect of the ventral horn (arrowhead) are labeled by retrogradely transported dextran conjugates, which also visualize axons projecting to the LC (arrow) (left panel). Motor neurons and axons labeled by tracer injection into the SC are located in the ventrolateral aspect of the motor horn (right panel). (B) Consecutive cryosections of the ventral horn showing backfilled neurons after injection of labeled dextran into the longus colli or the semispinalis cervicis muscle. Lhx3 marks MMC motor neurons. LC motor neurons are located in the medial aspect of the MMC and are expressing OC1. In situ hybridization against miR-9 shows that LC neurons do not express miR-9, in contrast to adjacent MMC neurons located more laterally. These lateral Lhx3^{+} MMC neurons are labeled after tracing SC projections but are not OC1-positive and they show enhanced miR-9 expression. NC = notochord, scale bar 20 μm.

SC muscle are located in the lateral aspect of the MMC (MMC_{SC}), which is devoid of OC1 but expresses high levels of miR-9 (Fig. 3B). Thus, our expression analysis in combination with retrograde tracing studies, revealed a mutually exclusive, pool-specific distribution pattern of OC1 and miR-9, suggesting a functional relationship.

miR-9 regulates Onecut1 expression

The 3′UTR of OC1 contains two miR-9 binding sites that are highly conserved in vertebrates (Fig. 4A). To test whether miR-9 is capable of regulating OC1 protein expression through these target sites, we generated a luciferase reporter construct containing 4 OC1 target sites (4x OC1ts) in the 3′UTR or the biological relevant cOC1-3′UTR (cOC1-UTR) downstream of the firefly luciferase coding sequence. When a miR-9 expressing plasmid was co-transfected into Hek293T cells together with one these two plasmids, luciferase activity was reduced by 40% (for 4x OC1ts) or 35% (for cOC1-UTR), compared to the luciferase activity in the absence of miR-9 (Fig. 4B). Expression of miR-9 had no effect on luciferase expression when OC1 target sites were absent from the 3′UTR of the pGL3 vector (Fig. 4B).

To explore whether miR-9 is capable of regulating OC expression in vivo, we overexpressed miR-9 in the chick spinal cord. Endogenously, the pre-miR-9 hairpin sequence generates not only the mature miR-9 microRNA, but also the antisense microRNA miR-9* (Lagos-Quintana et al., 2002). To avoid side effects arising from miR-9* expression, which is known to affect proliferation of neuronal progenitors in the spinal cord (Yoo et al., 2009), we used a pre-miR-9 precursor that is incapable of producing mature miR-9*. When pre-miR-9 was electroporated together with a GFP expressing plasmid, a strong miR-9 signal was detected only in the electroporated side of the

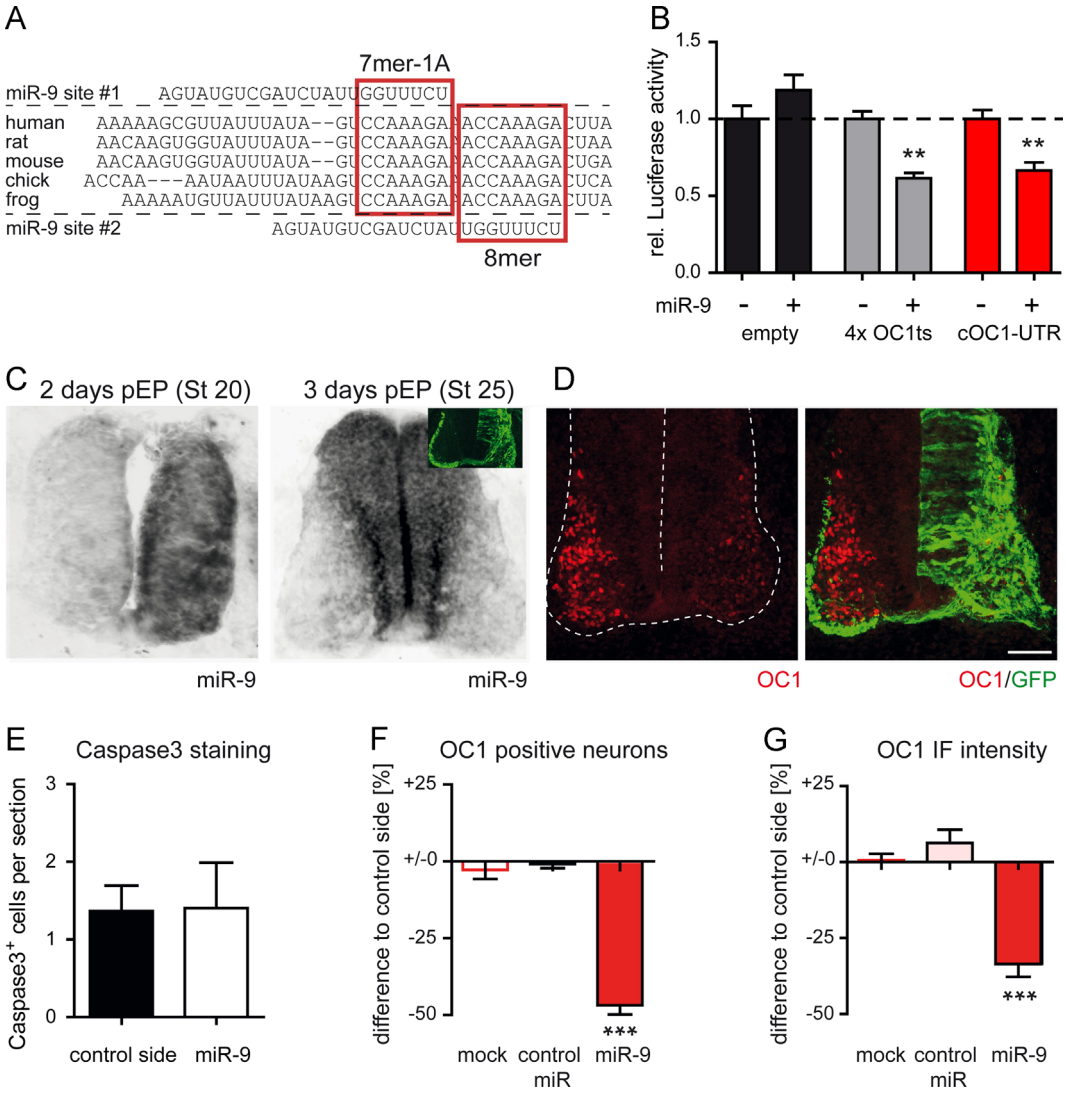

Fig. 4. miR-9 regulates OC1 expression. (A) Two highly conserved miR-9 binding sites (red boxed nucleotides) are found in the 3′ untranslated region of the OC1 gene. Seed sequences of miR-9 target sites show seed matches of 7mer-1A and 8mer, respectively, according to Targetscan6.0 (Friedman et al., 2009). (B) Luciferase assay with empty pGL3, pGL3 containing 4 OC1-miR-9 target sites in firefly luciferase 3′UTR (4x OC1ts) or the biologically relevant cOC1 3′UTR (cOC1 UTR). Co-transfection of HEK293T cells with 4x OC1ts or cOC1 UTR and a miR-9 expressing plasmid resulted in a significant reduction of relative Luciferase activity to 61.5% ± 3.4% or 66.5% ± 5.3% ($p < 0.01$, $n=6$), respectively. Firefly luciferase activity from the empty vector co-transfected with miR-9 was not affected significantly. (C) Electroporation of 5 μM pre-miR-9 miRNA precursor (Ambion) at HH St 12 into chick neural tube results in miR-9 overexpression in the right side of the spinal cord two days after electroporation (pEP; HH St 20/21). Note that hardly any endogenous miR-9 expression is detectable at this stage (left side of the spinal cord). Three days after electroporation, miR-9 expression in the electroporated half of the spinal cord (see inlet for co-electroporated GFP) is only weakly higher compared to the control side. (D) OC1 expression after co-electroporation of 5 μM pre-miR-9 and pCAG-GFP 3 days after electroporation. OC1 expression is significantly decreased compared to the control side. (E) Staining for activated Caspase3. Overexpression of miR-9 did not induce cell death in the electroporated side of the spinal cord (miR-9: 1.40 ± 0.59; control: 1.37 ± 0.33). (F) Quantification of OC1 expressing neurons. Compared to the non-electroporated side of each cryosection, miR-9 overexpression led to a significant loss of 46.1% ± 3.0% of OC1-positive cells ($n=28$ sections from 3 embryos, $p < 0.0001$). In contrast, mock EP (−2.0% ± 3.0%, $n=15/3$) or the negative control pre-miR (−0.1% ± 1%, $n=14/3$) did not change OC1 cell numbers significantly. (G) Quantification of OC1 immunfluorescence (IF) in OC1-positive neurons from electroporated side compared to control side on the same cryosection. After electroporation of pre-miR-9 the mean OC1 signal is decreased by 33.5% ± 4.2% ($n=28/3$, $p < 0.0001$). In contrast, mock EP (+0.6% ± 2.1%, $n=15/3$) or the negative control pre-miR (+6.3% ± 4.4%, $n=14/3$) did not change OC1 immunosignal significantly. Scale bar 50 μm.

Fig. 5. Overexpression of miR-9 induces changes in motor neuron subtype identity. (A–C) Immunostainings against Isl1/FoxP1, Hb9/Lhx1 and Lhx3/OC1 at HH St25 reveal motor columns at brachial spinal levels after electroporation of pCAG-GFP only (mock EP, left panels), a negative control sequence (middle panels), or pre-miR-9 (right panels). No difference in columnar distribution is observed in control conditions (mock EP and control pre-miR), in contrast, in miR-9 gain-of-function (pre-miR-9) situations, the numbers of LMCm neurons (asterisk) and Lhx3$^+$/OC1$^+$ MMC$_{LC}$ neurons (asterisk) are strongly reduced while the numbers of LMCl neurons are increased (asterisk). (D) Electroporation efficiency visualized by co-electroporated pCAG-GFP. (E) Quantification of numbers of Isl1$^+$/FoxP1$^+$ (LMCm), Lhx1$^+$/Hb9$^+$ (LMCl), Lhx3$^+$/Hb9$^+$ (MMC) and Lhx3$^+$/OC1$^+$ (MMC$_{LC}$) neurons was determined 4 days after electroporation (HH St 27/28), normalized to respective motor neurons in the non-electroporated side of the spinal cord and presented as the difference to control side. After electroporation of pre-miR-9, numbers of LMCm neurons are decreased by 48.4% ± 3.2 ($n=21$ sections of three embryos, $p < 0.0001$) while LMCl numbers are significantly increased by 36.3% ± 12.2 ($n=24/3$, $p < 0.001$). Electroporation of the CAG-GFP plasmid only (mock EP) or overexpression of a control pre-miR sequence does not significantly alter neuron numbers in the LMC or MMC. Evaluation of MMC neurons reveals no effect on total Lhx3$^+$/Hb9$^+$ motor neurons (+1.4% ± 10.7%, $n=16/3$, $p=1$), however, the amount of OC1$^+$/Lhx3$^+$ double-positive MMC$_{LC}$ neurons decrease significantly by 26.0% ± 7.8% ($n=32/3$, $p < 0.005$). (F) Electroporation of pre-miR-9 causes a small reduction of total FoxP1$^+$ cells (− 10.5% ± 4.9, $n=34/3$, $p=0.2$) when compared to the control side. This reduction is, however, not significant. Mock EP or overexpression of a control pre-miR sequence do not change the total number of FoxP1$^+$ cells. (G) Schematic drawing of the effects by miR-9 GOF. Scale bars 50 μm.

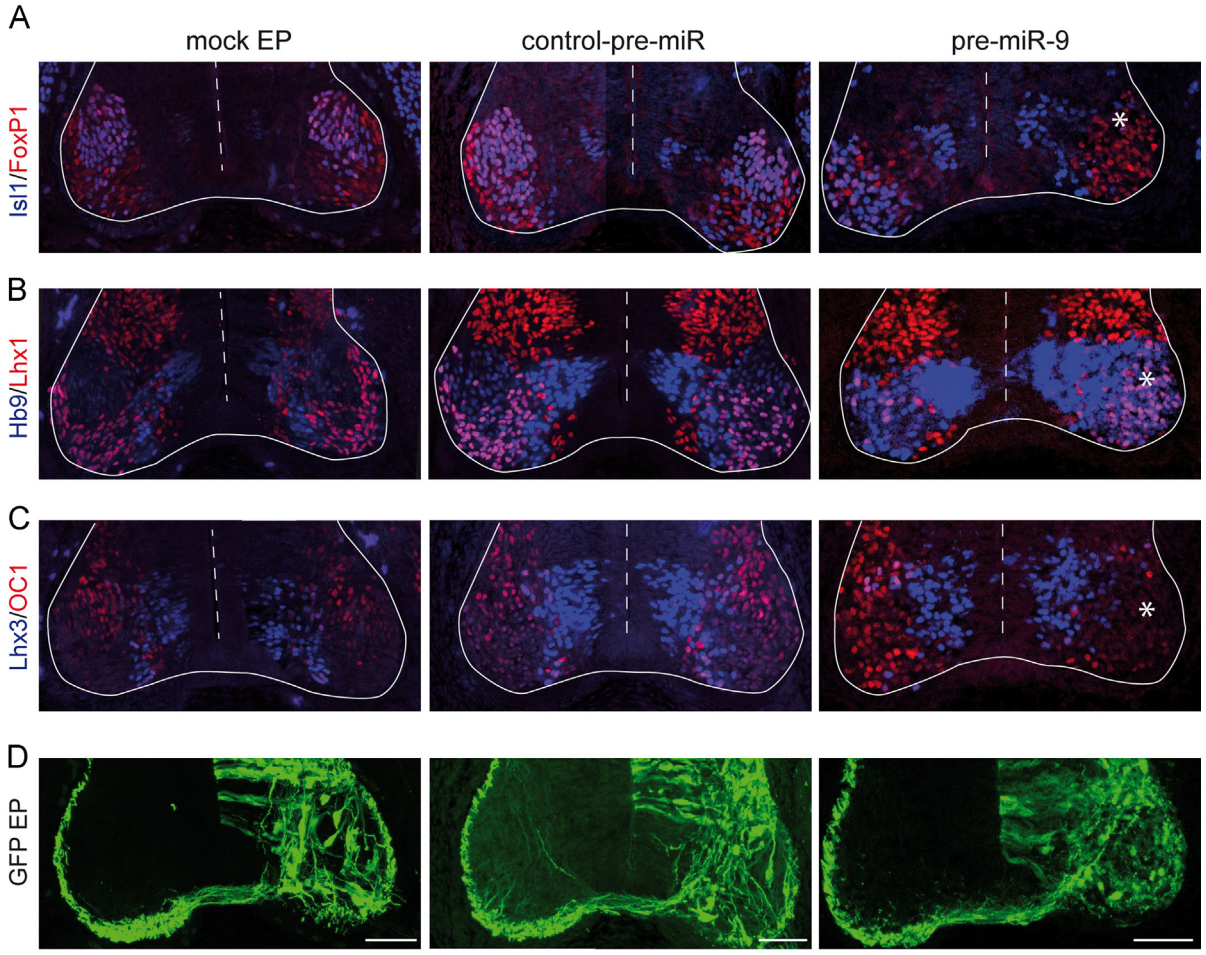
A
mock EP
control-pre-miR
pre-miR-9
Isl1/FoxP1
B
Hb9/Lhx1
C
Lhx3/OC1
D
GFP EP

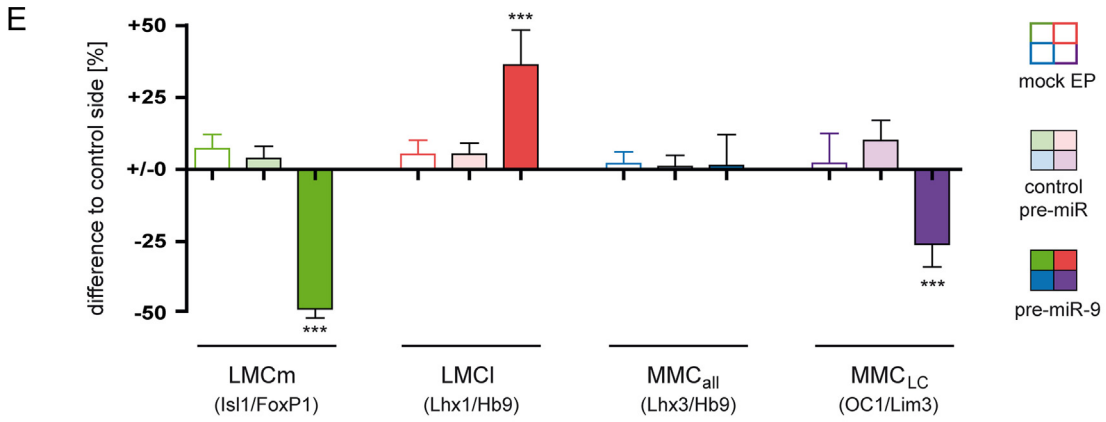
E
difference to control side [%]
+50
+25
+/-0
-25
-50
***
***
***
mock EP
control pre-miR
pre-miR-9
LMCm (Isl1/FoxP1)
LMCl (Lhx1/Hb9)
MMC all (Lhx3/Hb9)
MMC LC (OC1/Lim3)

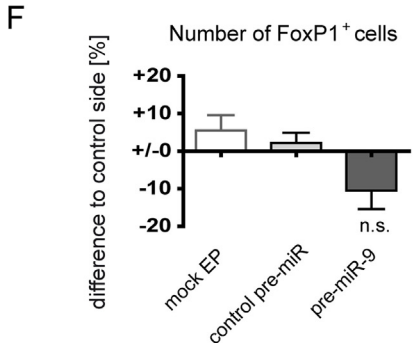
F
Number of FoxP1+ cells
difference to control side [%]
+20
+10
+/-0
-10
-20
n.s.
mock EP
control pre-miR
pre-miR-9

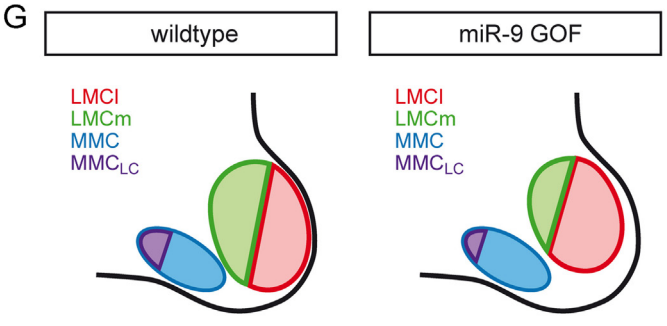
G
wildtype
miR-9 GOF
LMCl
LMCm
MMC
MMC LC

spinal cord (Fig. 4C), whereas almost no endogenous miR-9 was detectable at this developmental stage (HH St 21). This strong overexpression was downregulated at later stages despite a successful electroporation indicated by the co-expressed GFP (Fig. 4C).

Similar to previous observations (Otaegi et al., 2011), we saw no increase in cell death following miR-9 overexpression, as determined by activated Caspase3 staining (Fig. 4E). We then asked whether miR-9 gain-of-function has any impact on OC1 expression. We found a 50% reduction in the number of OC1-positive neurons in the ventral horn compared to the non-electroporated control side (Fig. 4D and F). In addition, the level of OC1 expression in OC1-positive neurons is also strongly decreased (Fig. 4G). No change in the number of OC1-expressing neurons nor in the level of OC1 expression was detected following electroporation of either the control pre-miR sequence or the expression of GFP alone. Our data show that miR-9 negatively regulates OC1 protein expression during chick spinal cord development.

Overexpression of miR-9 changes the subcolumnar composition of LMC and MMC

Next, we investigated the effect of miR-9 gain-of-function on the generation and organization of motor columns and pools. We found that at HH stage 28 the number of Isl1$^+$/FoxP1$^+$ LMCm neurons was reduced by almost 50% when compared to the non-electroporated side (Fig. 5A and E),while numbers of Lhx1$^+$/Hb9$^+$ neurons of the LMCl were significantly increased by one-third (Fig. 5B and E). Interestingly, the total number of Lhx3$^+$ MMC neurons was not altered, but a significant decrease in OC1/Lhx3 double-positive MMC$_{LC}$ neurons was observed (Fig. 5C and E). Mock electroporation, or electroporation of a negative control pre-miR sequence, did not result in a significant alteration of any cell numbers (Fig. 5E). The same effect was also evident already one day earlier at HH stage 25 (Fig. S2). Changes in FoxP1$^+$ cell numbers did not reach a significant level (Fig. 5F). Thus, our results show that overexpression of miR-9 during the maturation of spinal motor neurons leads to a reduction of neurons of the MMC$_{LC}$ and to a shift towards later-born lateral LMC neurons (Fig. 5G).

To test whether the generation of supernumerary LMCl neurons caused by overexpressing miR-9 also resulted in an increased number of dorsal axon projections, we examined the innervation of the chick wing using immunostaining against neurofilament in wholemount embryos. We measured the thickness of the dorsal (radial) and ventral (sum of ulnar and median) nerves at specific landmark points (Fig. 6B), and normalized these measurements to the thickness of respective nerves in the contralateral, non-electroporated side. Overexpression of

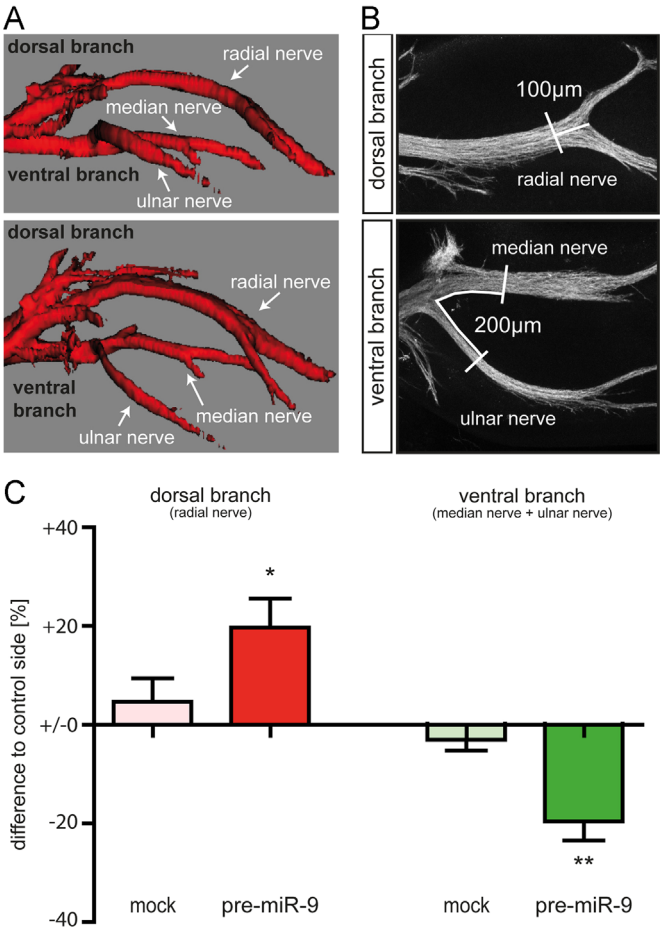

Fig. 6. miR-9 gain-of-function leads to decrease of ventrally projecting axon branches. (A) 3D visualization of axon branches innervating the chick wing in wholemount embryos stained for neurofilament at HH St 28. (B) Distinct landmarks, e.g. distinguished points where axonal branches split were used to determine the thickness of axon branches. Thickness of the radial nerve was determined 100 µm proximally to the split point while the thickness of the median and ulnar nerves was determined 200 µm distally to the split point. (C) Quantification of the branch thickness of electroporated dorsal (radial) and ventral (sum of median and ulnar) axon branches were determined for each embryo and normalized to respective axon branch thickness of the non-electroporated side. After mock electroporation no difference of wing innervation was observed (dorsal: $+4.7\% \pm 4.8\%$, $n=8$, $p=0.36$; ventral: $-3.1\% \pm 2.2\%$, $n=8$, $p=0.2$), but overexpression of miR-9 led to an increase of the dorsal axons branch ($+19.7\% \pm 5.9\%$, $n=9$, $p<0.05$) innervated by LMCl neurons, while the ventrally projecting axon branch was decreased by $19.6\% \pm 3.9\%$ ($n=9$, $p<0.005$) compared to the non-electroporated control side.

Fig. 7. Motor neuron specification is altered after miR-9 knock down. (A) The miR-9 sponge plasmid contains 18 bulged binding sites for miR-9, each separated by a 4 nucleotide long spacer sequence in the 3′ region of the GFP coding sequence and its expression is driven by the strong CAG promotor. (B) In a miR-9 sensor assay, the effective downregulation of luciferase activity by miR-9 ($30.6\% \pm 3.6\%$, $p<0.0001$, $n=3$) can be rescued with the miR-9 sponge ($81.4\% \pm 3.2\%$, $p=0.07$, $n=3$), while the scrambled sponge shows no effect ($34.3\% \pm 3.1\%$, $p<0.0001$, $n=3$). (C) Immunostainings at HH St 27 against columnar markers Isl1/FoxP1 (LMCm), Lhx1/Hb9 (LMCl) and Lhx3/OC1 (MMC$_{LC}$) on the non-electroporated side (control, left panels) and electroporated side of the spinal cord (electroporated, rights panels). (D) Quantification of miR-9 loss-of-function experiments. The numbers are shown as relative change of the electroporated side compared to the control side. miR-9 loss-of-function induces a significant increase of LMCm neurons by $36.6\% \pm 8.6\%$ ($p<0.001$, $n=23$ sections from four embryos), while the numbers of LMCl neurons are decreased by $15.0\% \pm 4.1\%$ ($p<0.01$, $n=23/4$). There is no significant change in total Lhx3$^+$ MMC neurons ($-4\% \pm 5\%$, $p=0.3$, $n=18/4$), but the numbers of OC1$^+$/Lhx3$^+$ double-positive MMC$_{LC}$ neurons are increased by $72.4\% \pm 22.5\%$ ($p<0.01$, $n=19/4$). (E) Determination of transcriptional profile of GFP expressing cells. In LMC neurons GFP expression resulting from miR-9 knockdown is almost exclusively seen in Isl1$^+$/FoxP1$^+$ medial LMC neurons ($97.7\% \pm 1.6\%$, $n=15/4$) but not in Lhx1$^+$/Hb9$^+$ lateral LMC neurons ($2.3\% \pm 1.6\%$, $n=15/4$). This differs significantly ($p<0.0001$) from LMC neurons electroporated with the empty vector (LMCm $47.5\% \pm 1.9\%$; LMCl $52.5 \pm 1.9\%$, $n=10/3$). In MMC neurons GFP expression resulting from miR-9 knockdown is much more evident in Lhx3$^+$/OC1$^+$ cells (MMC$_{LC}$: $66.5\% \pm 5.1\%$, $n=22/3$) than in the remaining Lhx3$^+$/OC1$^-$ MMC neurons (MMC$_R$: $33.5\% \pm 5.1$, $n=22/3$). Expression of the empty control vector leads to the opposite distribution of GFP$^+$ MMC neurons (MMC$_{LC}$: $22.3\% \pm 3.0\%$; MMC$_R$: $77.7\% \pm 3.0$, $p<0.0001$, $n=10/3$). (F) After electroporation of the sponge the changes in the total number of FoxP1$^+$ motor neurons do not reach significance ($+16.2\%$, $n=24/3$, $p=0.06$). (G) Quantification of OC1 immunfluorescence in GFP-positive motor neurons containing the miR-9 sponge sequence ($+$) or not ($-$). In miR-9 depleted motor neurons mean OC1 intensity is almost twice as high (54.5 ± 1.8, $n=814$ cells) as in motor neurons electroporated with the control plasmid (28.7 ± 2.2, $n=443$, $p<0.0001$). (H) Correlation between GFP and OC1 signal intensities. OC1 expression is positively correlated with GFP expression in miR-9 knock down motor neurons (linear regression: $y=0.2955x+26.658$, Pearson $r=0.35$, $n=958$, $p<0.0001$) while in contrast in the control experiment OC1 expression is negatively correlated with GFP expression (linear regression: $y=-0.0761x+33.42$, Pearson $r=-0.10$, $n=479$, $p<0.05$). a.u.=arbitrary units. (I) Illustration of the effects caused by miR-9 LOF. Scale bar 20 µm.

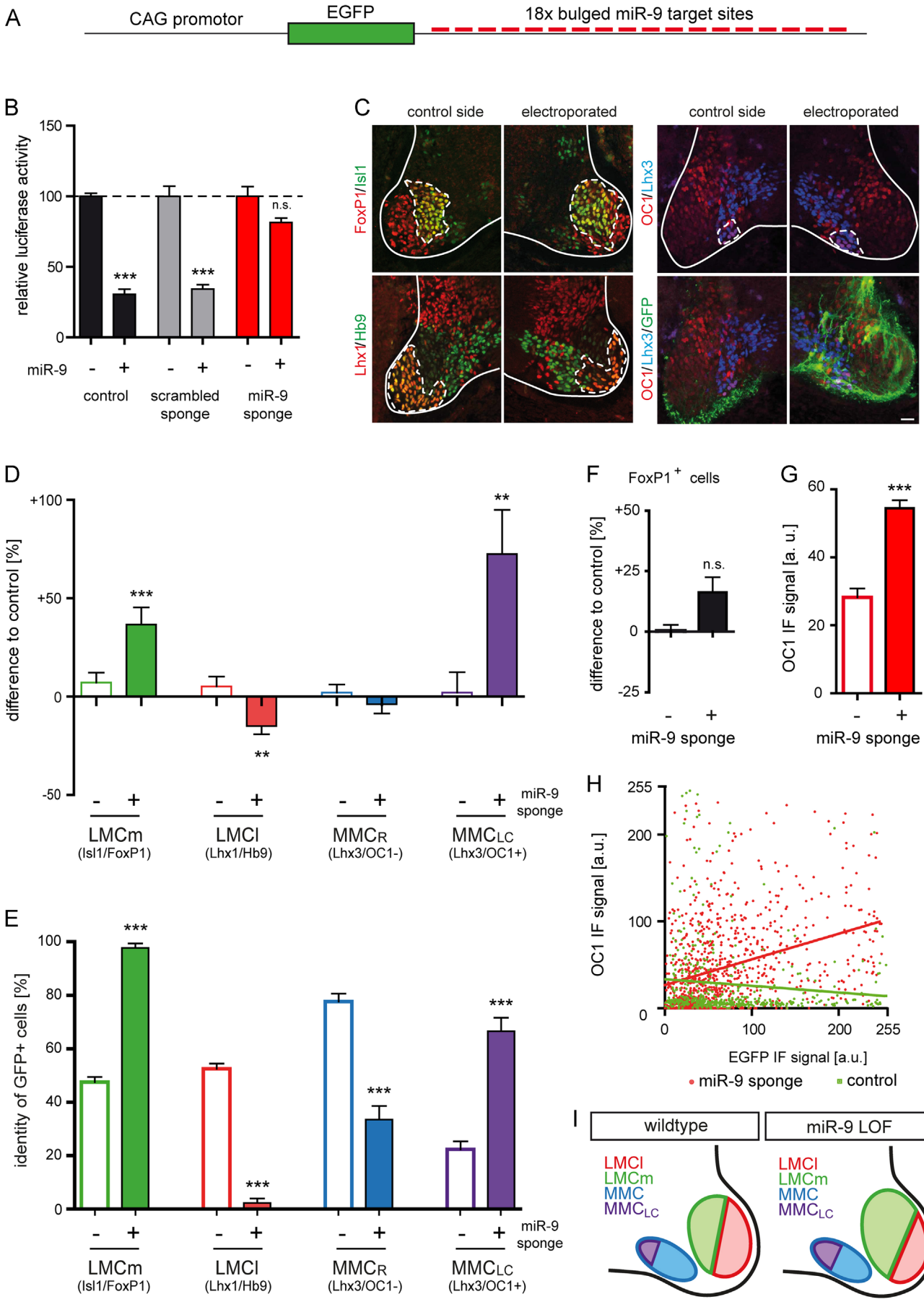
A
CAG promotor
EGFP
18x bulged miR-9 target sites
B
relative luciferase activity
150
100
50
0
***
***
n.s.
miR-9 - + - + - +
control
scrambled sponge
miR-9 sponge
C
control side
electroporated
control side
electroporated
FoxP1/Isl1
Lhx1/Hb9
OC1/Lhx3
OC1/Lhx3/GFP
D
difference to control [%]
+100
+50
0
-50
***
**
**
miR-9 sponge
LMCm (Isl1/FoxP1)
LMCl (Lhx1/Hb9)
MMCR (Lhx3/OC1-)
MMCLC (Lhx3/OC1+)
E
identity of GFP+ cells [%]
100
80
60
40
20
0
***
***
***
***
miR-9 sponge
LMCm (Isl1/FoxP1)
LMCl (Lhx1/Hb9)
MMCR (Lhx3/OC1-)
MMCLC (Lhx3/OC1+)
F
FoxP1+ cells
difference to control [%]
+50
+25
0
-25
n.s.
miR-9 sponge
G
OC1 IF signal [a. u.]
60
40
20
0
***
miR-9 sponge
H
OC1 IF signal [a.u.]
255
200
100
0
0
100
200
255
EGFP IF signal [a.u.]
miR-9 sponge
control
I
wildtype
miR-9 LOF
LMCl
LMCm
MMC
MMCLC
LMCl
LMCm
MMC
MMCLC

miR-9 led to an increased thickness of the dorsally projecting radial nerve, while in contrast the thickness of ventrally projecting nerves was decreased (Fig. 6C). When we expressed GFP only, no differences in the branch thickness of radial, ulnar or median nerves were found (Fig. 6C). These results demonstrate that the supernumerary lateral LMC neurons that are generated after overexpression of miR-9 exhibit LMCl identity also in their axonal projection patterns and follow the dorsal trajectory correctly into the wing.

From this we conclude that manipulation of motor neuron identity by varying miR-9 expression directly influences the size of particular motor neuron populations, but leaves the pathfinding capacities of the motor neurons generated under these conditions intact, resulting in corresponding alterations of nerve branch thickness.

miR-9 loss-of-function increases numbers of LMCm and MMC_{LC} neurons

Next, we functionally depleted endogenous miR-9 by electroporating a miR-9 "sponge plasmid" (miR-9 sponge) into the chick spinal cord (Fig. 7A). In order to test the specificity and efficiency of the plasmid we performed a luciferase-based miR-9 sensor assay in which the luciferase activity is strongly downregulated when miR-9 is expressed. The miR-9 sponge vector effectively rescued the luciferase activity to a normal level, while a scrambled sponge had no influence on this effect (Fig. 7B).

The effective sponge plasmid consist of 18 bulged miR-9 target sites located downstream of a GFP coding sequence (Fig. 7A). Translation of GFP is repressed as long as functionally active miR-9 is available in the electroporated cell. Thus, GFP fluorescence serves as a marker for a functional knockdown of miR-9 (Ebert and Sharp, 2010). While we found a significant reduction of Lhx1/Hb9 double-positive LMCl neurons when compared to the non-electroporated control side, the numbers of $Isl1^+/FoxP1^+$ neurons of the LMCm were strongly increased (Fig. 7C and D). Total numbers of $FoxP1^+$ motor neurons were slightly increased, however, this trend did not reach significance (Fig. 7F). Electroporation of a control plasmid (GFP only) did not cause a change in numbers nor in the distribution of lateral and medial LMC neurons. We next investigated whether the identity of MMC neurons is also changed upon miR-9 knock down. We found a strong increase in $OC1^+/Lhx3^+$ MMC_{LC} neurons that is not observed in control situations while the total numbers of $Lhx3^+/Hb9^+$ MMC neurons remained unchanged (Fig. 7C and D). Together, these results complement our data on miR-9 gain-of-function and demonstrate that endogenous miR-9 is involved in the correct establishment of subcolumnar motor neuron identity.

While electroporation of a GFP control plasmid resulted in an even distribution of GFP^+ neurons in the entire LMC, GFP^+ cells were not homogenously distributed within the ventral horn after electroporation of the miR-9 sponge (Fig. 7C). To determine which motor neuron subtypes express GFP and therefore are depleted of miR-9, we examined the transcriptional identity of GFP^+ cells. After miR-9 knock down, almost all GFP^+ LMC neurons were $Isl1^+/FoxP1^+$ (98%), whereas virtually no $GFP^+/Lhx1^+/Hb9^+$ cells were observed (Fig. 7E). This indicates that lateral but not medial LMC neurons depend on functionally active miR-9. When we analyzed $GFP^+/Lhx3^+$ MMC neurons under control conditions, the majority (78%) did not co-express OC1 resembling the endogenous ratio between MMC_{SC} and MMC_{LC} neurons. However, after miR-9 knock down, two-thirds of $GFP^+/Lhx3^+$ MMC neurons co-expressed OC1 indicating that the generation of MMC_{LC} neurons is independent of miR-9 function (Fig. 7E).

Thus, OC1 is strongly downregulated due to the silencing function of exogenous miR-9. We hypothesized that blocking miR-9 by electroporating a miR-9 sponge should lead to higher levels of OC1 in GFP^+ neurons. We therefore determined OC1 intensity in GFP^+ motor neurons electroporated with the miR-9 sponge or control plasmid. We found that the mean OC1 expression level in GFP^+ neurons that are functionally depleted of miR-9 is almost twice as high as in control neurons expressing GFP only (Fig. 7G). Next, we investigated whether GFP and OC1 expression levels are correlated after miR-9 knockdown. We found a positive correlation of OC1 and GFP levels in individual neurons if miR-9 was functionally blocked while a negative correlation was observed in control situations (Fig. 7H). This indicates that the decrease of OC1 expression depends on functionally active miR-9.

Together, our miR-9 loss-of-function analyses revealed that the early-born, OC1 expressing brachial motor pools, LMCm and MMC_{LC}, gain in number (Fig. 7I) and their generation is independent on miR-9 functionality. This instructive capacity of miR-9 is most likely mediated through the inhibition of OC1, since its expression is enhanced when miR-9 is knocked down.

Discussion

miR-9 and Onecut1 are expressed in mutually exclusive patterns

The transcriptional networks orchestrating motor neuron subtype specification are tightly controlled, both at spatial and temporal levels. We show here that microRNA-9 plays an essential role in mediating the switch from early-born to late-born motor neuron populations through the regulation of OC1 protein expression.

OC1 expression in the developing chick spinal cord is present in virtually all mature motor neurons in the early phase of motor neuron migration (HH St 18), while it is restricted to subpopulations of motor neurons in the LMC and MMC after completion of the phase of motor neuron generation (around HH St 29) (Francius and Clotman, 2009). We found that the restriction of OC1 expression to particular subsets of motor neurons coincides with the generation of columnar divisions. OC1 is expressed in early-born motor neurons of the LMCm and the MMC_{LC} that both innervate ventral muscle groups, namely ventral wing musculature and the longus colli muscle, respectively. Late-born neurons that migrate to the lateral aspects of the LMC and MMC showed very low or no OC1 expression. In contrast, expression of miR-9 was high in LMCl neurons and even more prominent in MMC_{SC} neurons. It is these motor neurons that are born the latest in the brachial spinal cord and that innervate the semispinalis cervicis muscle, which is located dorsal to the spinal cord (Fig. 8A). The dynamic expression pattern of miR-9, with expression starting after HH St 19 in the chick spinal cord and at comparable developmental stages in the mouse, has also been reported by others (Bell et al., 2004; Chen and Wichterle, 2012; Darnell et al., 2006; Zheng et al., 2010). Different from a previous study that reported a uniform distribution of miR-9 in the LMC at HH St 24 and its downregulation at HH St 29 (Otaegi et al., 2011), we find a differential expression of miR-9 also at late stages such as HH St 28–30 (Figs. 1 and 3). This is in line with a recent study that showed strong miR-9 expression at comparable ages in mouse embryos (E13.5, Chen and Wichterle, 2012). Since such discrepancies may arise due to different staining protocols, we sought to verify our expression data by an independent experimental approach using a sensor construct to detect miR-9 activity cell autonomously. Indeed, we detected an increased activity of miR-9 in lateral LMC neurons compared to LMCm. This result strongly supports our observation of a differential miR-9 expression within the LMC.

Inhibition of OC1 by miR-9 is an important component of motor neuron specification

miRNAs can execute their repressive nature in two ways: either directly by inhibiting protein translation, or indirectly by reduc-

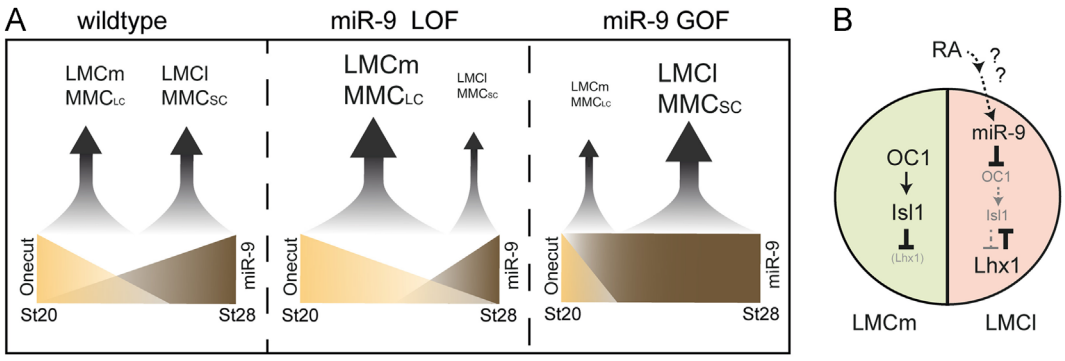

Fig. 8. Functional interactions of miR-9 and Onecut1 leading to a proper generation of spinal motor neurons. (A) Model of the temporal development of brachial motor column in dependence of Onecut1 and miR-9 expression levels. (B) Schematic illustration of the signaling cascade leading to proper specification of LMC divisions.

ing mRNA stability, but in both cases miRNAs eventually cause a reduction of target protein levels. This makes it likely that a particular miRNA and its direct target protein display non-overlapping expression patterns (Bartel and Chen, 2004). miR-9 is therefore expressed at the right time and location to constitute a *bona fide* candidate of a regulator of OC1 protein. This notion is also supported by the presence of miR-9 target sites in the 3′UTR of OC1 mRNA (Fig. 4A; (Dajas-Bailador et al., 2012), the direct repression of OC1 by miR-9 in vitro (Fig. 4B), as well as in vivo: overexpression of miR-9 in the spinal cord decreased the number of OC1$^+$ motor neurons and the OC1 expression level within these neurons dramatically (Figs. 4E and 5B).

Proper function of the spinal motor system depends on the generation of appropriate numbers of distinct subtypes of neurons and their assembly into functional circuits. During development, motor neurons establish a topographic projection to limb musculature whereby the cell body position in the LMC predicts the trajectory of the corresponding axon: motor neurons located in the medial LMC innervate ventral limb muscles whereas lateral LMC neurons project to dorsal limb targets (Jessell, 2000). The establishment of medial and lateral divisions of the LMC is controlled by a network of secreted factors and transcriptional regulators that leads to cross-repressive interactions and finally to a mutual exclusion of Isl1 and Lhx1 expression domains (Kania and Jessell, 2003). During the establishment of LMC divisional identity, retinoids secreted from early-born LMCm neurons are essential to induce extinction of Isl1 expression and initiate expression of Lhx1 in the later-born prospective lateral LMC neurons (Sockanathan and Jessell, 1998; Sockanathan et al., 2003). Indeed, the high expression levels in the progenitor zone might indicate an early function of miR-9 in maturation of motor neuron subsets. Also, a miR-9 binding site is predicted in the 3′UTR of Isl1 suggesting a possible regulation of Isl1 through miR-9. However, we and others did not find a direct interaction between miR-9 and Isl1 (own unpublished observations and Lagos-Quintana et al., 2002).

We found that overexpression of miR-9 strongly reduces OC1 protein levels in the developing chick spinal cord. In addition, we observed a decrease in the numbers of LMCm neurons and an increase in LMCl neurons. The LMCm-promoting activity of OC1 is corroborated by a recent study in transgenic mice showing that OC1 acts upstream of Isl1 and directly stimulates its expression in specific motor neuron subtypes. In OC1/2 double knockout mice no Isl1$^+$ LMCm neurons are generated but instead all LMC neurons adopt the fate of LMCl neurons, as indicated by Lhx1 expression and projection to dorsal limb musculature (Roy et al., 2012). Since Isl1 expression in early post-mitotic motor neurons is not affected in OC1/2 knockout mice, this strongly suggests that OC transcription factors are important to support the maintenance of Isl1 expression in LMCm neurons at later stages thus preventing them from adopting an LMCl fate. We cannot exclude that miR-9 also has an effect earlier in development, however, our data suggest a direct effect on OC1 expression levels in postmitotic neurons that influences the consolidation of motor pools. This is also in line with our observation that OC1 expression is strongly decreased or even absent in Lhx1$^+$ LMCl neurons that express high levels of miR-9. Silencing OC1 during motor neuron development might be essential to allow for the downregulation of Isl1 in LMC neurons. Subsequently, expression of Lhx1 can be initiated, since the repressive activity of Isl1 has been relieved.

How might miR-9-OC1 interactions fit into the regulatory network that determines spinal motor neuron fate decisions during development? A recent study described binding sites for CEBP-α and CEBP-β transcription factors in the promotor regions of all three genes encoding miR-9 precursors (Kutty et al., 2010) and all-trans-retinoic acid has been shown to induce these transcription factors (Masaki et al., 2006). In the same study, 4HPR, a synthetic derivative of retinoic acid, was shown to induce strong miR-9 expression in retinal pigment epithelium cells (Kutty et al., 2010). These results and our observations in the present study support a model of a signaling pathway in which retinoids secreted from early-born LMCm neurons could induce miR-9 expression in later-born LMCl neurons. Subsequently, miR-9 inhibits OC1 expression and thus also Isl1 expression in these prospective LMCl neurons. This enables the later-born motor neurons to initiate Lhx1 expression and subsequently adopt the LMCl fate (Fig. 8B).

miR-9 fulfills multiple functions in the establishment of motor neuron pools

Besides OC1 miR-9 has additional predicted and experimentally validated target genes, affecting diverse neurodevelopmental processes from neuronal differentiation, regulation of axon extension and branching to apoptosis (Bejarano et al., 2010; Dajas-Bailador et al., 2012; Laneve et al., 2010). Recently, miR-9 has been shown to target and silence FoxP1 and thereby fine-tune the levels of FoxP1 protein in motor neurons (Otaegi et al., 2011). Using a promoter-driven approach a very strong miR-9 overexpression was achieved in later-born motor neurons at HH St 24. This late miR-9 gain-of-function lead to a decrease of FoxP1 levels and LMC neuron numbers and a concomitant increase of MMC neuron numbers. We have used an experimentally different approach that overexpressed miR-9 already in progenitor and early post-mitotic motor neurons, resulting in an early silencing of OC1 and consecutively in a decrease of early-born motor neurons such as LMCm and MMC$_{LC}$ neurons. Since we employed a “pulsed” miR-9 overexpression with fading intensities in later-born motor neuron populations such as LMCl and MMC$_{SC}$, we likely do not interfere in the events consolidating the identity of these motor neurons. Thus, our findings and previous reports support the emerging view that microRNAs together with transcriptional regulators act

spatially and temporally in concert at different levels of neuronal differentiation, specification and maturation.

In summary, we have shown that miR-9 controls OC1 expression in the developing spinal cord in a spatially and temporally dynamic pattern coinciding with the differentiation of motor neuron subtypes of the LMC and the MMC. Experimentally manipulating miR-9 expression levels shifts the balance between medial and lateral LMC divisions in a way that is consistent with a direct induction of Isl1 through OC1. Finally, our results provide a plausible model integrating the early inductive capacity of retinoic acid and the cross-repressive events between Isl1 and Lhx1 that result in the generation of motor neuron specificity.

Acknowledgements

We thank T. Haehl and N. Perl for technical assistance; A. Kolodkin, C. Broesamle and the members of the Huber lab for critical reading and comments to the manuscript.

Appendix A. Supporting information

Supplementary data associated with this article can be found in the online version at http://dx.doi.org/10.1016/j.ydbio.2013.12.023.

References

Bartel, D.P., Chen, C.Z., 2004. Micromanagers of gene expression: the potentially widespread influence of metazoan microRNAs. Nat. Rev. Genet. 5, 396–400.
Bejarano, F., Smibert, P., Lai, E.C., 2010. miR-9a prevents apoptosis during wing development by repressing *Drosophila* LIM-only. Dev. Biol. 338, 63–73.
Bell, G.W., Yatskievych, T.A., Antin, P.B., 2004. GEISHA, a whole-mount in situ hybridization gene expression screen in chicken embryos. Dev. Dyn. 229, 677–687.
Bonev, B., Pisco, A., Papalopulu, N., 2011. MicroRNA-9 reveals regional diversity of neural progenitors along the anterior–posterior axis. Dev. Cell. 20, 19–32.
Chen, J.A., Wichterle, H., 2012. Apoptosis of limb innervating motor neurons and erosion of motor pool identity upon lineage specific dicer inactivation. Front. Neurosci. 6, 69.
Dajas-Bailador, F., Bonev, B., Garcez, P., Stanley, P., Guillemot, F., Papalopulu, N., 2012. microRNA-9 regulates axon extension and branching by targeting Map1b in mouse cortical neurons. Nat. Neurosci..
Darnell, D.K., Kaur, S., Stanislaw, S., Konieczka, J.H., Yatskievych, T.A., Antin, P.B., 2006. MicroRNA expression during chick embryo development. Dev. Dyn. 235, 3156–3165.
Tonelli, De Pietri, Calegari, D., Fei, F., Nomura, J.F., Osumi, T., Heisenberg, N., Huttner, W.B., C.P., 2006. Single-cell detection of microRNAs in developing vertebrate embryos after acute administration of a dual-fluorescence reporter/sensor plasmid. Bio.Tech. 41, 727–732.
Ebert, M.S., Sharp, P.A., 2010. Emerging roles for natural microRNA sponges. Curr. Biol. CB 20, R858–861.
Francius, C., Clotman, F., 2009. Dynamic expression of the Onecut transcription factors HNF-6, OC-2 and OC-3 during spinal motor neuron development. Neuroscience 165, 116–129.
Friedman, R.C., Farh, K.K., Burge, C.B., Bartel, D.P., 2009. Most mammalian mRNAs are conserved targets of microRNAs. Genome Res. 19, 92–105.
Gutman, C.R., Ajmera, M.K., Hollyday, M., 1993. Organization of motor pools supplying axial muscles in the chicken. Brain Res. 609, 129–136.
Huber, A.B., Kania, A., Tran, T.S., Gu, C., Garcia, De Marco, Lieberam, N., Johnson, I., Jessell, D., Ginty, T.M., Kolodkin, A.L., D.D., 2005. Distinct roles for secreted semaphorin signaling in spinal motor axon guidance. Neuron 48, 949–964.
Jessell, T.M., 2000. Neuronal specification in the spinal cord: inductive signals and transcriptional codes. Nat. Rev. Genet. 1, 20–29.
Kania, A., Jessell, T.M., 2003. Topographic motor projections in the limb imposed by LIM homeodomain protein regulation of ephrin-A:EphA interactions. Neuron 38, 581–596.
Kutty, R.K., Samuel, W., Jaworski, C., Duncan, T., Nagineni, C.N., Raghavachari, N., Wiggert, B., Redmond, T.M., 2010. MicroRNA expression in human retinal pigment epithelial (ARPE-19) cells: increased expression of microRNA-9 by *N*-(4-hydroxyphenyl)retinamide. Mol. Vis. 16, 1475–1486.
Lagos-Quintana, M., Rauhut, R., Yalcin, A., Meyer, J., Lendeckel, W., Tuschl, T., 2002. Identification of tissue-specific microRNAs from mouse. Curr. Biol. CB 12, 735–739.
Laneve, P., Gioia, U., Andriotto, A., Moretti, F., Bozzoni, I., Caffarelli, E., 2010. A minicircuitry involving REST and CREB controls miR-9-2 expression during human neuronal differentiation. Nucleic Acids Res. 38, 6895–6905.
Lau, P., Verrier, J.D., Nielsen, J.A., Johnson, K.R., Notterpek, L., Hudson, L.D., 2008. Identification of dynamically regulated microRNA and mRNA networks in developing oligodendrocytes. J. Neurosci. 28, 11720–11730.
Masaki, T., Matsuura, T., Ohkawa, K., Miyamura, T., Okazaki, I., Watanabe, T., Suzuki, T., 2006. All-trans retinoic acid down-regulates human albumin gene expression through the induction of C/EBPbeta-LIP. Biochem. J. 397, 345–353.
Otaegi, G., Pollock, A., Hong, J., Sun, T., 2011. MicroRNA miR-9 modifies motor neuron columns by a tuning regulation of FoxP1 levels in developing spinal cords. J. Neurosci. 31, 809–818.
Plaisance, V., Abderrahmani, A., Perret-Menoud, V., Jacquemin, P., Lemaigre, F., Regazzi, R., 2006. MicroRNA-9 controls the expression of Granuphilin/Slp4 and the secretory response of insulin-producing cells. J. Biol. Chem. 281, 26932–26942.
Roy, A., Francius, C., Rousso, D.L., Seuntjens, E., Debruyn, J., Luxenhofer, G., Huber, A. B., Huylebroeck, D., Novitch, B.G., Clotman, F., 2012. Onecut transcription factors act upstream of Isl1 to regulate spinal motoneuron diversification. Development 139, 3109–3119.
Shi, Y., Zhao, X., Hsieh, J., Wichterle, H., Impey, S., Banerjee, S., Neveu, P., Kosik, K.S., 2010. MicroRNA regulation of neural stem cells and neurogenesis. J. Neurosci. 30, 14931–14936.
Sockanathan, S., Jessell, T.M., 1998. Motor neuron-derived retinoid signaling specifies the subtype identity of spinal motor neurons. Cell 94, 503–514.
Sockanathan, S., Perlmann, T., Jessell, T.M., 2003. Retinoid receptor signaling in postmitotic motor neurons regulates rostrocaudal positional identity and axonal projection pattern. Neuron 40, 97–111.
Tsuchida, T., Ensini, M., Morton, S.B., Baldassare, M., Edlund, T., Jessell, T.M., Pfaff, S. L., 1994. Topographic organization of embryonic motor neurons defined by expression of LIM homeobox genes. Cell 79, 957–970.
Yoo, A.S., Staahl, B.T., Chen, L., Crabtree, G.R., 2009. MicroRNA-mediated switching of chromatin-remodelling complexes in neural development. Nature 460, 642–646.
Zheng, K., Li, H., Zhu, Y., Zhu, Q., Qiu, M., 2010. MicroRNAs are essential for the developmental switch from neurogenesis to gliogenesis in the developing spinal cord. J. Neurosci. 30, 8245–8250.